Third Year Literature Report
by
Felix Fernandez-Alonso

State-selective Spectroscopies in Surface Dynamics

Supervisor: Dr. D. O. Hayward

Table of contents

Without doubt lasers have revolutionised almost every area of science and molecular reaction dynamics is by no means an exception. During the seventies and early eighties groups led by Levine, Bernstein or Zare, to mention just a few, applied laser spectroscopic techniques to the study of chemical reactions in the gas phase [1,2,3]. For the first time, the energy partitioning of the products could be measured directly. It provided an invaluable amount of information about the redistribution of energy in the course of reactions and allowed meaningful conclusions to be drawn about their mechanisms.

Application of these techniques to surface science came in the early eighties [4,5,6,7]. The first applications were made to simple scattering and desorption experiments on surfaces using very simple molecules (i.e. NO, H_2). In the past ten years, there has been a continuous growth of the field and as of today a few experiments on simple chemical reactions on surfaces (i.e. photodissociation) has been possible.

The key tool used in these experiments is the laser, acronym for Light Amplification by the Stimulated Emission of Radiation. Essentially, laser radiation is characterised for having the following properties [8]:

-wavelength tunability
-high intensity
-short (controllable) duration of radiation
-monochromaticity
-spatial coherence

A complete classification of all laser spectroscopic techniques is not trivial. Depending on the type of interaction of light with the atom or molecule of interest, one could differentiate between linear and non-linear laser spectroscopies. The former is based on single quantum linear interaction of the laser light with the particle of interest. The latter corresponds to a non-linear single-quantum or multi-quantum interaction of laser light. In practice, linearity is present at low laser intensities while non linearity requires high laser fluences.

The classification presented above is very convenient for introducing the techniques discussed here: laser-induced fluorescence (LIF) and resonance-enhanced multiphoton ionisation (REMPI). LIF is a linear process while REMPI is an inherently non-linear one. Historically, LIF was introduced before REMPI in the analysis of internal state distributions. At the beginning of the past decade, multiphoton ionisation (MPI) was a very fresh subject while LIF was being used extensively in the study of the dynamics of gas-phase reactions [9,11]. The application of multiphoton ionisation to product state analysis was held back by the need to accumulate a body of information analogous to the spectroscopic data base that underlied LIF. However, many features of MPI predicted a promising future for this technique (i.e. greater sensitivity and wider applicability than LIF).

The first chapter will discuss in some detail the idiosyncrasies of these two techniques, their advantages and disadvantages as well as how a proper internal-state analysis should be carried out by the experimentalist. The remaining sections describe the

most recent advances in the field, focusing in the last four years. The reader interested in reviewing the literature before 1988 will be referred to the appropriate literature cited therein.

1. State-selective spectroscopies.

1.1 Laser-induced fluorescence (LIF).

1.1.1 Basic features.

In LIF, laser radiation is used to promote a molecule to an excited electronic state whose emission is then detected by conventional means (i.e. a photomultiplier). Laser radiation is so selective that only specific rovibronic levels of the ground state will be excited to the upper state and subsequently their emission detected [10]. Figure 1 summarises this process. A spectrum of the fluorescence intensity versus wavelength, the so-called excitation spectrum, can be used to obtain the relative populations of these different rovibronic states. A detailed analysis of the intensity features and how populations might be obtained is not a trivial matter and will be discussed later in this section.

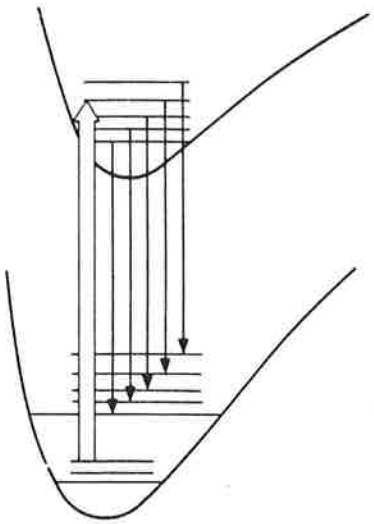

Fig. 1 Diagram showing the fluorescence process. The molecule is first excited by means of a laser. LIF is concerned with the decay from such excited state (reprint from ref. 10).

Resolution in a LIF experiment depends upon two factors: the nature of absorption bands and the spectral characteristics of the laser. A candidate for LIF analysis must have appreciably populated states from which absorption lines within the wavelength range of the laser can originate. Also, the spectrum needs to be sufficiently resolved to allow identification of the levels participating. It is necessary to have accurate relative line

strengths, whose determination becomes very difficult if they are not available directly from experiment.

All these prerequisites impose some obvious limitations on the applicability of the technique. On the one hand, not all molecules fluoresce efficiently and vibrational and rotational band strengths, the Frank-Condon and Höln-London factors, are known for a large but limited set of simple polyatomics [11].

The hydroxyl radical is a good example of a species well suited for LIF studies. Its spectrum has an open structure allowing easy resolution of individual features (fig.2).

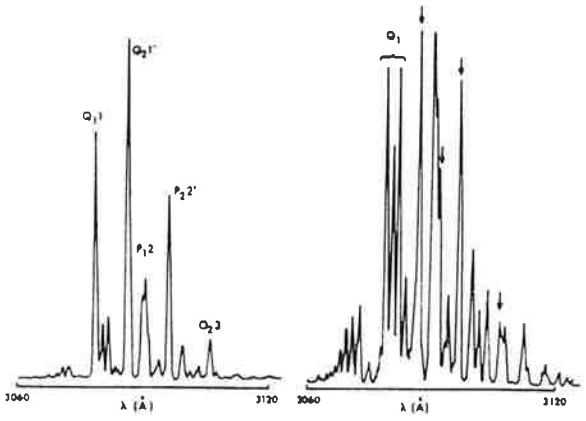

Fig. 2 LIF spectrum of an OH radical. The scans correspond to the (0,0) band of the $A^2\Sigma$-$X^2\Pi$ system (reprint from ref. 10).

1.1.2 Analysis of fluorescent intensities.

In a very simplified analysis of LIF spectra, the relative band intensities display the relative vibrational or rotational populations of ground state molecules as shown below,

$$N_{\upsilon''\upsilon'} \alpha \; I_{\upsilon''\upsilon'} \qquad (1)$$

Unfortunately this simple relationship holds in only a few cases and under very special experimental conditions. Unlike simple absorption spectra, fluorescence has a nontrivial polarisation dependence. In early work on quantum theory of dispersion of radiation Breit [12] established the foundations of this dependence in the form of an expression known as the Breit formula [13]. It is not possible in this brief survey of LIF to deal with the complete form of the Breit formula. Under most operating conditions the population of a ground electronic state $N_{\upsilon''}$ can be related to the intensity of the υ'' to υ' transition via the expression shown below,

$$N_{\upsilon''} = I_{\upsilon'\upsilon''} / \{q_{\upsilon'\upsilon''} \rho(\upsilon'\upsilon'') \Sigma_{\upsilon} (v^4_{\upsilon'\upsilon} q_{\upsilon'\upsilon})\} \qquad (2)$$

where $q_{\upsilon'\upsilon''}$ is the Frank-Condon factor for the υ'' to υ' transition, $\rho(\upsilon'\upsilon'')$ is the laser power density and the summation is over all the vibrational states υ of the ground electronic state to which the particular υ' state fluoresces [14]. Equation (2) requires a knowledge of $q_{\upsilon'\upsilon''}$ and therefore good spectroscopic data on the excited and ground state potential energy surfaces. In favourable cases, i.e. very similar ground and electronic states, expression (2) can be reduced to (1) and a measurement of relative intensities will yield a good estimate of the relative vibrational populations of the ground state.

Similar remarks apply to the analysis of rotational lines, if resolvable. In this case, it would be necessary to use the appropriate Höln-London factors if the problem cannot be reduced to its simplest form.

1.1.3 Effects of saturation.

In many cases the ultimate goal of an LIF experiment is to detect the relative populations of ground state rotational and vibrational levels. In recent years, it has been realised that an accurate determination of relative populations requires an understanding of how the fluorescence signal changes with the polarisation of incident and detected photons [15]. Furthermore, the assumption that the excited state population is linearly proportional to laser intensity fails as the laser power increases, the relationship becoming increasingly sublinear. This effect is generally called saturation.

Theoretically, the dependence of LIF intensity on polarisation is treated by using directional Einstein coefficients which are used to model the interaction of directional, polarised radiation with molecules having a specific orientation. The specifics of the theoretical treatment are quite involved. It is concluded that intensities and populations are related by the following expression:

$$I = K' n B_{12} \Delta t_L \qquad (3)$$

where K' depends on the characteristics of the detector as well as on the relative orientation of the molecular dipole with respect to the electric field vector of both the absorbed and emitted photons. Δt_L is the duration of the rectangular laser pulse. For equation (3) to hold, the polarisation of the laser and the detected fluorescence need to be constant during the experiment, the molecular distributions of all states probed must be similar and the fractions of collected fluorescence due to the Q and P or R branches have to be the same for all states probed. In general, equation (3) is only valid in the limit of low laser power. As the power laser increases, non-linear behaviour becomes predominant and the following expression must be used:

$$\frac{n_i}{n_j} = \frac{I_i \int \frac{\left[\sum_{l=0}^{\infty} a^j_{2l} P_{2l}(\cos\theta)\right] a^j_{21} b^j_{12} \rho^j \{1 - \exp[-(2b^j_{12}\rho^j + A^j_{21})\Delta t_L]\}}{2b^j_{12}\rho^j + A^j_{21}} d\Omega}{I_j \int \frac{\left[\sum_{l=0}^{\infty} a^i_{2l} P_{2l}(\cos\theta)\right] a^i_{21} b^i_{12} \rho^i \{1 - \exp[-(2b^i_{12}\rho^i + A^i_{21})\Delta t_L]\}}{2b^i_{12}\rho^i + A^i_{21}} d\Omega.} \qquad (4)$$

In this very complex expression, the a's and b's are the aforementioned directional Einstein coefficients. This illustrates how complicated matters may become in a very rigorous treatment of the problem. Fortunately, in many cases saturation might leave LIF spectra unchanged (i.e. all Frank-Condon factors are roughly the same) and even improve the signal to noise ratio [16]. However, in probing features whose relative line strengths differ significantly, saturation can seriously alter the appearance of spectra. In order to avoid such complications, the experimentalist just concerned with extracting relative populations should bear in mind the effects of saturation on LIF spectra and at best attempt to avoid such complications by operating at low laser fluences.

1.1.4 Internal-state distribution analysis.

Figure 3 below shows a typical set-up of a LIF detection system. The Nd:YAG laser is used to induce photodesorption on the surface. The photodesorbed products are analysed with an excimer-pumped tunable laser which runs parallel to the surface. In this specific experiment the laser was tuned to 224 nm for the state-specific, single-photon LIF detection of desorbed NO molecules [17]

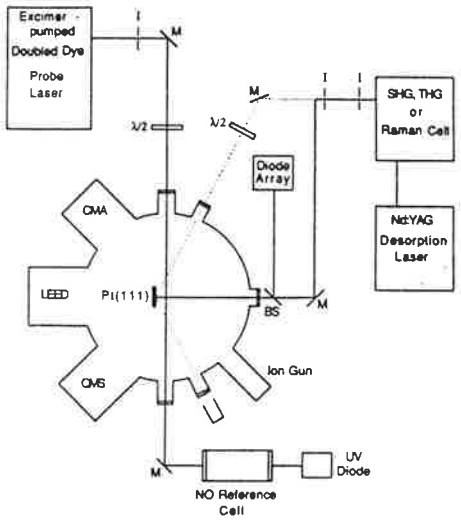

Fig. 3 Laser-induced desorption/ LIF apparatus. The dotted line represents the excitation laser while the solid line corresponds to the LIF beam, running perpendicular to the surface (reprint from ref. 17).

Appropriate tuning of the probe laser wavelength for 226.8 and 224.4 nm allows the determination of rotational (J), spin-orbit (O) and lambda doublet (Λ) populations in the υ=0 and υ=1 vibrational bands by pumping the (0,0) and (1,1) bands of the $A^2\Sigma^+$-$X^2\Pi_0$ transition. The ground electronic state of NO has two spin orbit states with the F_2, O = 3/2 being 124 cm^{-1} above the F_1, O = 1/2 level.

After passing through the UHV chamber, the probe laser enters a reference cell which contains a dilute mixture of NO. The NO reference cell allows wavelength

calibration. The probe laser beam passes parallel to, and a set distance away from the surface (4.0 mm approximately).

With this experimental set-up it is possible to obtain time-of-flight (TOF) spectra of NO molecules in specific quantum states by setting the probe laser resonant with appropriate rovibronic transitions and electronically varying the time delay between the desorption and probe laser pulses. Velocity-specific rovibronic excitation spectra can be obtained by monitoring the LIF intensity signal at a fixed time delay while scanning the probe laser wavelength through the NO (0,0) or (1,1) band absorption regions.

The rotational state populations within each vibrational level are obtained by dividing the measured LIF intensities by the appropriate Höln-London factor. These internal state distributions are generally analysed in terms of a Boltzmann plot in which the naperian logarithm of the population is plotted versus the energy of each state. In the case of rotational populations, the population needs to be divided by the degeneracy of each rotational state, i.e. (2J+1). A linear correlation will be indicative of a Boltzmann distribution with the slope proportional to the characteristic rotational temperature. Deviations from linearity will be indicative of populations not at thermal equilibrium. Also, any differences between the rotational and vibrational temperatures of products and reactants will be useful in the elucidation of the mechanisms of energy transfer that occurred on the surface. Fig. 4 below shows several Boltzmann plots corresponding to three different desorption-laser wavelengths. Additionally, the rotational state distribution within each spin-orbit level deviates from a Boltzmann form for wavenumbers less than 300 cm^{-1}, while above 300 cm^{-1} the population falls off exponentially with a slope on the Boltzmann plot of 226±15 °K for the F_2 state and 251±20 °K for the F_1 state.

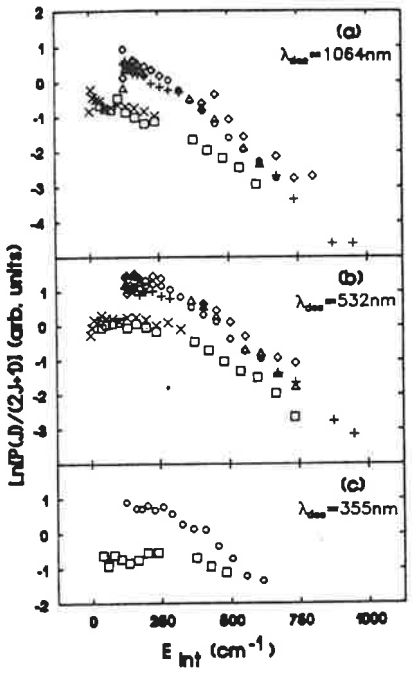

Fig. 4 Boltzmann plots for different laser desorption wavelengths. Note the non-Boltzmann behaviour below 300 cm^{-1} (reprint from ref. 17).

1.2 Resonance-enhanced multiphoton ionisation (REMPI).

In recent years, the Resonance-Enhanced Multiphoton Ionisation technique has gained in popularity with respect to LIF mainly because of an increased amount of theoretical work in the field of non-linear spectroscopies. Population analysis of REMPI spectra is possible if a sufficient account is taken of effects such as saturation and intermediate state alignment. This section attempts to provide a brief and simplified account of how REMPI is used in the detection of internal state distributions. Unfortunately, REMPI is fairly recent and no standard textbook provides an accessible description of the technique. This section will describe briefly its essential features and then explain in a rather qualitative way how the experimentalist might be able to extract internal state distributions.

1.2.1 Essential features.

REMPI falls in the category of non-linear, multistep excitation spectroscopies [18]. The simplest scheme to consider in a multiphoton process is a two-photon absorption. The first photon takes the molecule to a real or virtual excited state. The second photon promotes the molecule to an even higher electronic state which might be above the ionisation limit [19].

Just to illustrate how different multiphoton processes are from the conventional one-photon ones, let us consider their selection rules. Selection rules for a multiphoton excitation are distinctive depending on the number of photons involved in the transition [20]. Keeping the simple scheme of a two-photon process described above, selection rules are the same as for vibrational Raman transitions. In terms of group theory, the appropriate direct product must contain the totally symmetric irreducible representation, that is:

$$T(\varphi_{e'})T(S_{ij})T(\varphi_{e''}) = A \text{ (or contain A)}, \qquad (5)$$

where $T(\varphi_{e'})$ is the symmetry of the upper state $T(\varphi_{e''})$ is the symmetry of the ground state and $T(S_{ij})$ are the elements of the two-photon tensor, equivalent to $T(\alpha_{ij})$ where α_{ij} is the polarisability tensor. In the case of vibronic transitions it is necessary to consider both the symmetries of the electronic ground and vibrational wavefunctions coupled together and apply the same arguments discussed before.

In general there are two distinct monitoring procedures. In both cases a tunable laser is scanned through an absorption system. For a two-photon transition, if two photons match the energy gap to an excited state, fluorescence might be detected from that state. The intensity of total, undispersed fluorescence as a function of laser frequency gives the desired two-photon excitation spectrum. An alternative way is to use two initial photons to take the molecule into a state of higher energy and then a third photon to ionise it. This is called a (2+1) multiphoton ionisation spectrum. If in addition, the intermediate states are eigenstates and not virtual states of the molecule the technique is called **R**esonance-**E**nhanced **M**ulti**P**hoton **I**onisation (REMPI). (2+1) and (1+1) spectra are the two most common cases. Once the molecule is ionised the number of ions collected is counted as a

function of laser frequency to produce a multiphoton ionisation spectrum. This technique, for example, is advantageous when the fluorescence quantum yield is too small for the method of multiphoton fluorescence spectroscopy.

1.2.2 Characteristics of the photoionisation method.

In most cases, photoionisation is the method of choice in the detection of small quantities of atoms and molecules. Amongst its most important advantages with respect to conventional spectroscopies one could cite the following [21]:

-high sensitivity, allowing the detection of single atoms or molecules during a single laser pulse.
-spectral resolution, governed by the multistep excitation linewidth of molecules or atoms which in turn depends on the individual linewidth of each excitation step.
-time resolution, possible in the course of a single irradiation event whose duration is shorter than the lifetime of each of the excited states (i.e. for molecules is in the order of a few nanoseconds).
-high selectivity, since multiple selective excitations at each step produces a sharp decrease in the probability of overlap with other transitions.
-universality, because in principle the technique is applicable to any atom or molecule. However, lack of suitable excitation lines in the UV-vis region might make detection difficult.

Multiphoton techniques have been used extensively in the past twenty years for the detection of minute concentrations of atoms. Andreyev et al. in 1975 and Letothov et al. in 1976 conducted the first experiments with molecules. However, **M**ulti**P**hoton **I**onisation spectra (MPI) of molecules poses a few complications. Selectivity is generally reduced due to the more complex character of the excited state of polyatomic molecules. Furthermore, molecules in intermediate excited states can undergo different photophysical or photochemical transformations which compete with photoabsorption and photoionisation. Photoionisation also creates a new problem namely that of the need of a mass-spectrometric technique of analysis to differentiate between the various types of ionisation products. Finally, molecular photoabsorption cross sections are generally small and it becomes necessary to use more powerful sources of radiation.

1.2.3 Multiphoton ionisation spectra of molecules.

The following prerequisites are essential in order to record a two-photon spectra of a molecule [21]:

(1) Achieve saturation of the first transition, which requires a laser fluence at least equal to that required for saturation. In general, this is done by using powerful pulses of radiation shorter than the lifetime of the excited state. Equation (6) shows this relationship:

$$\Phi 1(\upsilon_1) > \Phi 1sat \ \alpha \ 1/(2\sigma_{exc}) \quad (6)$$

where σ_{exc} is the cross section of the excited state and $\Phi(\upsilon_1)$ the laser fluence.

(2) Ionisation from the excited state requires the laser fluence of the laser to be greater than the power needed to saturate the ion state.

$$\Phi_2(\upsilon_2) > \Phi_{1sat} \ \alpha \ 1/(2\sigma_{ion}) \quad (7)$$

This generally requires an energy fluence $\Phi_2(\upsilon_2)$ of 0.1-1 J/m^2 or , equivalently, a light intensity of 10^{10}-10^{11} W/cm^2.

(3) Mass-Spectroscopic detection of the photoions. It is achieved with a time-of flight (TOF) apparatus which allows the recording of the entire mass spectrum for a single laser pulse.

The two-photon ionisation spectrum is determined by the dependence of the photoionisation yield on the frequency of laser radiation. Far from saturation, the ion yield from a two-step ionisation in the absence of relaxation of the intermediate state can be approximated by the following formula:

$$N_i = N_{exc} \sigma_{ion} \Phi_2(\upsilon_2) = N_o \ q \ \sigma_{exc} \Phi 1(\upsilon_1) \sigma_{ion} \Phi_2(\upsilon_2) \quad (8)$$

N_o is the number of molecules in the irradiated volume, q is the fraction of molecules interacting with the exciting radiation at frequency υ_1, $\Phi 1$ and Φ_2 are the energy fluences and σ are the cross sections for the excited and ion states. σ_{exc} determines the excitation spectrum of molecules while σ_{ion} depends on both the specific excited electronic-vibrational level and the excess energy of the two photons above the ionisation limit.

Unfortunately, this is a highly idealised case. Typical cross sections for multiphoton processes are generally 10^{-50} cm^4sec for a two-photon absorption and decrease dramatically as the number of photons increases. As a consequence, high light fluxes are needed in order to achieve a significant transition probability (i.e. 10^5 watts in 10^{-8}-second pulses) [22].

At the laser powers mentioned above, no transition can be considered in isolation, that is to say, all possible excitation pathways (ionisation, photodissociation, radiationless transitions, etc), must be considered. An appropriate rate analysis of a multiphoton process shows that at low laser intensities the overall ionisation probability to the ionisation continuum is simply proportional to the product of the cross sections and the intensity raised to the power of the number of photons involved in the transition. Thus, for a (m+n) multiphoton process:

$$\text{Ionisation probability} \ \alpha \ \sigma_i \sigma_{ii} I^{(m+n)} \quad (9)$$

At moderate intensities, the ionisation step is saturated and the overall probability is proportional just to $\sigma_i I^m$, where n is the number of photons involved in the first transition [22].

A series of line-broadening effects derived from the use of high laser intensities includes geometric saturation, lifetime broadening and the AC Stark effect. Polarisation effects have also proved to be important. The next section considers some of these effects and refer to different experimental and theoretical ways to deal with them.

1.2.4 Analysis of REMPI spectra and reduction of line intensities to population distributions.

It is the aim of this section to give a semiquantitative description of how to use REMPI spectra in internal-state distribution analysis. The (1+1) REMPI of the NO $A^2\Sigma$-$X^2\Pi$ system will be used as our model. Figure 5 shows the basic features of the multiphoton ionisation process of this molecule. NO has been widely used in surface scattering and surface desorption experiments and will be encountered in sections to follow [23,24].

A detailed theoretical analysis is far from simple and in many cases experimentalists have resorted to extracting population information after running a calibration REMPI with known samples thought to have a Boltzmann distribution. A more rigorous treatment of the problem should include both saturation and intermediate state alignment effects. The latter can be thought of in the following way. When a beam of linearly polarised light is incident on an isotropic distribution of ground state molecules (all M sublevels within a J level are equally populated), the intermediate state will be effectively aligned through a preferential excitation of those molecules having larger projections of the transition dipole moment on the electric field vector of the linearly polarised light beam. Ionisation efficiency might be M dependent and thus the anisotropy created in the intermediate state can affect the overall MPI ion yield.

The (1+1) REMPI process can be explained in terms of the system of rate equations shown in figure 6.

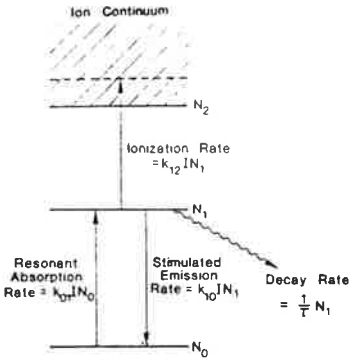

$$\frac{dN_0(t)}{dt} = -k_{01}I\,N_0(t) + k_{10}I\,N_1(t),$$

$$\frac{dN_1(t)}{dt} = k_{01}I\,N_0(t) - \frac{N_1(t)}{\tau} - k_{10}I\,N_1(t) - k_{12}I\,N_1(t),$$

$$\frac{dN_2(t)}{dt} = k_{12}I\,N_1(t).$$

Fig. 5.6 Schematic diagram of the (1+1) REMPI for NO and system of differential equations of the process (reprint from ref. 25).

Assuming the contribution from spontaneous emission is negligible and that the laser pulse is rectangular with amplitude I and temporal width Δt, the system of differential equations shown above can be solved exactly. Its solution is shown below.

$$N_2(\Delta t) = NF_{sat}(k_{01},k_{12},I\Delta t) \qquad (10)$$

Thus, the ion yield is proportional to the ground state population N and a saturation function which depends not on the laser intensity but on the area under the pulse. The constants k_{01}, k_{12} can be evaluated using a classical or quantum approach. A complete description of these theoretical treatments is out of place; the reader is referred to reference 25 for a complete coverage of the topic. Remarkably enough, both classical and quantum approaches yield very similar results.

The conclusions obtained above can be used in the analysis of the REMPI spectra of NO and ultimately lead to the extraction of internal-state distributions. Experimentally, the following steps need to be followed [26]:

(1) Record the 'isopower spectra', which includes recording the ion yields as a function of laser wavelength in such a way that all the ion intensities correspond to the same effective integrated spectrum.
(2) Correct the 'isopower spectra' in order to account for saturation and intermediate state alignment.
(3) Extract relative rotational population distributions within a given vibrational level.

In the first step REMPI spectra are recorded at different laser intensities. The behaviour of the spectra with the laser intensity varies for each resolved band and sometimes even across a single line profile. Figures 7 and 8 show the REMPI spectra of NO.

It is also necessary to check whether the photoions are just a consequence of resonant two-photon absorption. This is generally achieved by recording a photoelectron spectrum. In general, resonant ions will have no vibrational excitation while ions produced via other processes, for example, coherent two-photon transition will be vibrationally excited.

The isopower REMPI spectra now needs to be corrected for laser power changes. This involves normalising the spectra and requires a knowledge of ion signal power dependence. This behaviour is described by equation (10). A non-linear least-squares program is able to find the best coefficients for N, k_{01} and k_{12}. In most cases, k_{12} does not change significantly over the intensity range so that the problem is reduced to finding the best fit of N and k_{01} for a particular rovibronic transition.

The final extraction of populations needs a further correction for the interdependent effects of saturation and intermediate state alignment. The former is generally dominant at low laser intensities while the latter is important at high intensities.

Considering linearly polarised light, $\Delta M=0$ transitions will be allowed and a given transition is a sum of $(2J+1)$ independent transitions. Therefore, each spectral transition is a sum over independent transition probabilities for each M sublevel. Thus, there are M-independent rate constants we can use along with equation (10) to calculate ionisation efficiencies for a particular transition as the sum of the contributions for each M channel. A satisfactory expression for the population is given by equation (11).

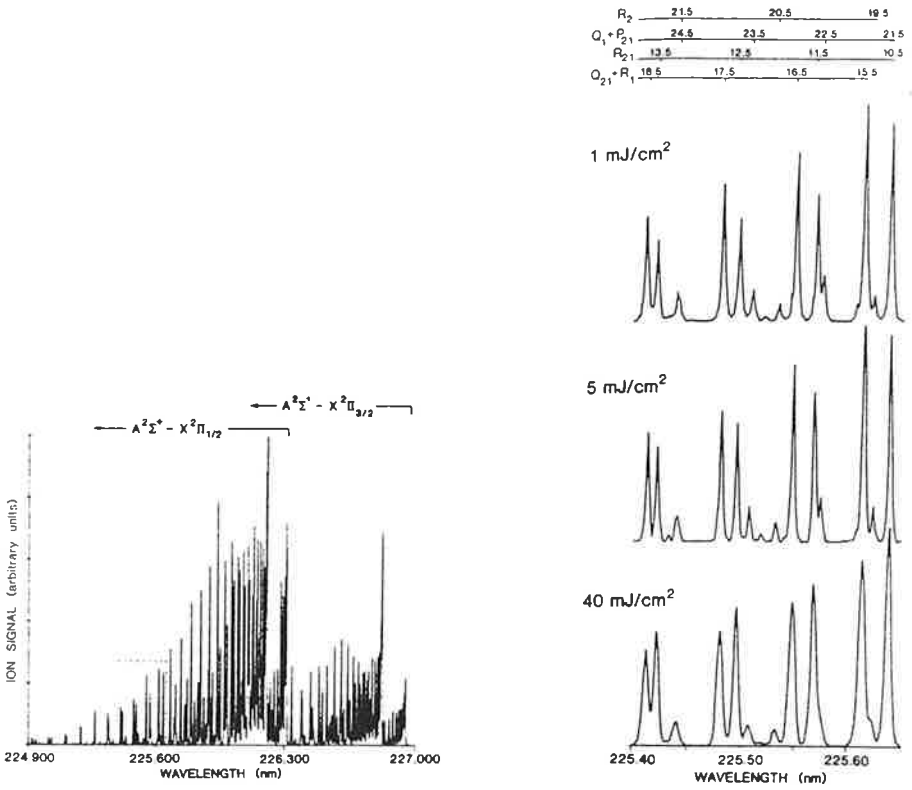

Figs. 7.8 (1+1) REMPI spectrum of the NO $A^2\Sigma$-$X^2\Pi$ band. Figure 8 shows expanded portions of the spectra recorded under isopower conditions (reprint from ref. 26).

$$N(J) = N_2\Delta t/\Sigma\{MF_{sat}(k_{01}(M),k_{12}(M),I\Delta t)\} \qquad (11)$$

The explicit forms of the rate constants $k_{01}((M)$ and $k_{12}((M)$ can be checked in reference 26. They involve a series of proportionality constants which might be evaluated from either ab initio calculation or experiment, the latter being more common.

As we have already seen in the chapter on LIF, population distributions at thermal equilibrium are represented using a Boltzmann plot. Figures 9 and 10 show the corrected and uncorrrected isopower spectra for the different branch contributions from the REMPI spectrum. It is clear from these two figures that accounting for both saturation and intermediate state alignment yields less uncertainty in the plots hence a better resolved characteristic rotational temperature.

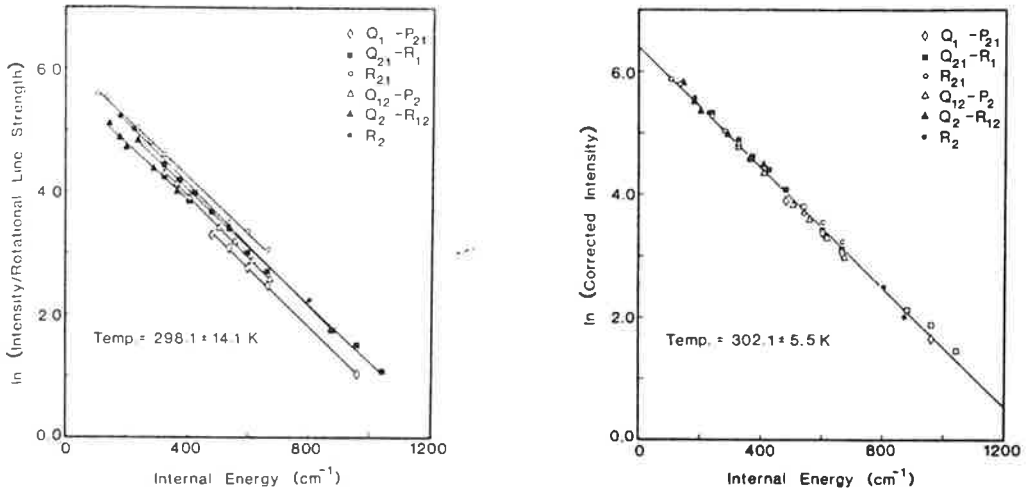

Figs. 9.10 Corrected (right) and uncorrected (left) Boltzmann plots. Corrections include the combined effects of intermediate state alignment and saturation as explained in the text (reprint from ref. 26).

2. Recent state-selected surface studies.

This section will focus on the most recent results, primarily those reported between 1988 and 1992. Where there is a need to resort to older literature, the reader will be referred to various review articles that cover the topic(s) in greater detail [27-29,31,60]

The section is divided into three subsections covering the most important areas that use LIF and REMPI as primary tools. These are: inelastic scattering and trapping/desorption; recombinative desorption; and laser and electron induced desorption.

The essence of all these experiments is not difficult to grasp. In inelastic scattering, molecules of a supersonic molecular beam with well-defined velocity, rotational and vibrational energy distributions are scattered from a surface under ultrahigh vacuum conditions. Different degrees of freedom within the molecule redistribute their energy and also exchange energy with the surface. In recombinative desorption, the molecules (generally hydrogen or one of its isotopic analogues) are initially adsorbed dissociatively onto the surface and then desorbed, normally by thermal means. This process is of great importance since it involves the recombination of atoms to form a chemical bond. It is therefore a very simple model to understand the basic dynamics of surface chemical reactions. Finally, the laser or electron induced desorption involves a change in the excitation source (i.e. a laser or an electron beam). Consequently, one would expect totally different mechanisms to be important under these regimes of highly concentrated excitation.

2.1 Inelastic scattering, trapping and desorption.

2.1.1 NO/Ag(111).

The NO/Ag(111) system is a good example of a weak molecule-surface interaction (12-20 kJ/mol) [32], ideal for direct-inelastic scattering experiments. The first studies of this sort were conducted by Zare et al. [33-34]. Several studies have been published since then [35-40]

In general, it was found that the average rotational energy increased linearly with surface temperature and that the binding energy was approximately 8 kJ/mol higher for $NO(X^2\Pi_{1/2})$ than for $NO(X^2\Pi_{3/2})$). Surprisingly enough, these observations could be qualitatively explained using the 'hard cube model' of Nichols et al. [41]. In this simple model, the surface is totally uniform and molecules undergoing a single collision with the surface are treated like ellipses with both rotational and translational energy.

Perhaps, the most remarkable feature was the presence of rotational rainbows characterised by a distinct non-Boltzmann hump at high J. The spin-orbit temperature was found to be similar to the rotational temperature for low J but it diverged to infinity at high J indication of the equipartition of population between the $^2\Pi_{1/2}$ and the $^2\Pi_{3/2}$) states. Λ-doublet populations, however, were preferentially populated with the π orbital perpendicular to the rotational axis. Studies on rotational polarisation indicated that for high J the intensity of LIF spectra varied strongly with the angle of polarisation of linearly polarised light showing that the scattered products were predominantly polarised with respect to the surface normal. Rotational excitation could then be explained by invoking the hard sphere model in which translational-to-rotational energy transfer occurs via collisions with the surface by forces acting normal to it [41].

The degree of vibrational excitation has also been measured [42]. Vibrationally excited molecules increased proportional to surface temperature and incident beam energy. Highly non-Boltzmann rotational populations were found, resembling those of the lowest vibration state. Theoretical models could reproduce appropriately most of the aforementioned features. They were unable, however, to predict the degree of rotational polarisation [43].

Recently, highly state-selected measurements of NO on Ag(111) for a wide range of incidence translational energies and angles from the surface normal have been performed. NO detection was achieved by the already standard (1+1) multiphoton ionisation method. The novel aspect of the experiment was the introduction of a supersonic molecular beam to study the scattering with well defined initial rotational populations [44].

Rotational state distributions were consistent with previous studies not only on the NO/Ag(111) [45] but also on the N_2/Ag(111) [46]. There was also an overall agreement in this respect with the theoretical models proposed [47], including the presence of a rotational rainbow at a beam energy of 0.85 eV (see fig. 11). However, it was not possible to observe the predicted supernumerary rainbows, probably due to the effects of surface corrugation.

In this same experiment angular distributions were all broad, characteristic of inelastic scattering, with the angle displaced in the supra-specular direction with increasing incident energy or J and decreasing surface temperature, indicative of momentum transfer between the surface and the scattered molecules. Shifts in angle were attributed to the imbalance between parallel and perpendicular momentum transfer. However, contrary to previous experiments and theoretical predictions, it was observed that parallel momentum was far from being conserved during scattering (i.e. energy transfer depended on incidence angle). At grazing angles most of the translational energy lost in the collision was converted to rotational excitation. The amount of energy transferred for higher incidence angles was smaller, indicative of a coupling of the translational energy of NO with surface phonons.

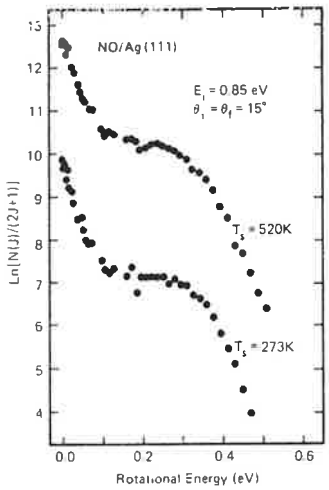

Figs. 11 Boltzmann plots of NO scattered from Ag(111). Notice the rotational rainbow present at low rotational energy, characteristic of this system (reprint from ref. 44).

In an experiment using a NO molecular beam, Tenner et al. [48] have correlated the reflection angle with the orientation of NO desorbing from Ag(111). At low incidence angles (i..e 15°) they observed rotational rainbows, in agreement with the first studies of this system [38]. At larger incidence angles (45°), two different contributions, a supraspecular and a subspecular, appeared yet only the supraspecular had rotational rainbows. These results could be fitted to an expression of the form shown below:

$$R_J = 2(I^-_{J'J} - I^+_{J'J})/(I^-_{J'J} + I^+_{J'J}) \qquad (12)$$

In this equation $I^-_{J'J}$ is the intensity obtained for the J-J' transition for a NO molecular beam with molecules preferentially aligned with the oxygen end pointing towards the surface and $I^+_{J'J}$ is the intensity obtained for a beam with the nitrogen end pointing towards the surface. In general, they found that for high J states, the desorption yield was larger for those molecules impinging the surface with the oxygen end while the

opposite was true for low J (approx. J<8.5). These observations corroborate the importance of orientation-dependent rotational excitation in scattering processes.

2.1.2 NO/Pt(111).

This system is an example of a strong molecule-surface interaction. It has a large binding energy (105-149 kJ/mol) yet it does not dissociate. It is therefore an ideal case for the study of both inelastic scattering and trapping/desorption dynamics.

Prior to 1989, a number of studies of the NO/Pt(111) system had been reported [49-56,58]. From the scattering experiments [49-52,58] it was found that rotational populations had well-characterised Boltzmann distributions. At low surface temperatures, the characteristic rotational temperature (T_r) was similar to the surface temperature (T_s) but at high T_s, $T_r<T_s$. The high NO coverage suggested that a trapping/desorption mechanism was operative. The difference between T_r and T_s observed at high T_s was termed 'rotational cooling in desorption'. The interaction mechanism changed if the surface was covered with oxygen [52]. Now, inelastic scattering became predominant. Further state-resolved measurements showed that the translational degree of freedom was accommodated most efficiently, the opposite being true for rotations. Temperature-programmed desorption (TPD) experiments showed two distinct peaks with different rotational temperatures and an isotropic distribution of angular momenta [58]. The model generally accepted at that time was that desorption occurred via a freely rotating state with weak coupling between the rotational and desorbing degrees of freedom. Rotational cooling was caused by rotation-to-translation energy transfer which suggested the existence of a loose physisorbed state for desorption from a strong chemisorbed bond.

Zare et al. [55] have conducted a series of very elegant experiments in which they report the first observation of rotational alignment in molecular desorption. REMPI spectra were used to extract accurate relative populations and alignment factors. Separate experiments with light perpendicular and parallel to the surface permitted the determination of not only populations but also of quadrupole moments, which can be related to the orientation of nitric oxide on the surface.

Inelastic scattering was studied in the range from 375 to 475 °K. Rotational distributions were non-linear only at low energies, the rotational temperature increasing along with the surface temperature. Figures 12 and 13 show the alignment data. At approximately J=25.5, the quadrupole moment reaches a minimum at -0.5. Both rotational distributions and quadrupoles were independent of doublet occupancies.

Trapping/desorption was achieved via firing a laser pulse 200μs after completion of the nozzle pulse. Each doublet showed identical behaviour but quadrupole moments increased monotonically for J>12.5 until reaching a positive value.

These findings suggested that for inelastic scattering, molecules with rotational quantum number above the beam energy are thermally accommodated with well-defined rotational temperatures. Surface vibrations were probably responsible for this high rotational excitation. Additional contributions were, if any, due to localised interactions of NO with surface atoms rather than a delocalised phonon-mediated energy transfer.

Rotational alignment in both inelastic scattering and trapping/desorption showed preferential alignment. For desorption, quadrupoles near 2 suggested a helicopter-type

motion. Quadrupoles near -1 were indicative of cartwheel motion (see fig. 14). Surface corrugation and other effects such as breakage of cylindrical symmetry made these quadrupoles appear at values below the expected.

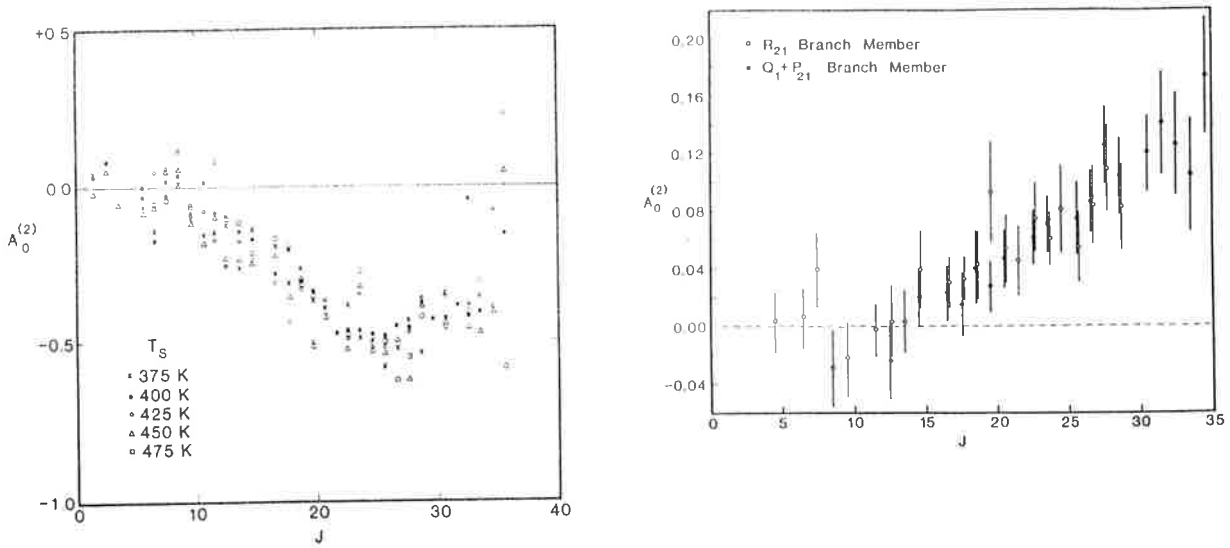

Figs. 12.13 Quadrupole moment alignment distribution as a function of rotational quantum number for both inelastic scattering (left) and desorption (right) (reprint from ref. 55).

Rotational alignment similar to this had been found before for the NO/Ag(111) system [57]. While the scattering process could still be explained in terms of a bouncing process of the NO 'cartwheel' with the surface, the observed alignment observed for desorption could not be reconciled with this picture. It seemed necessary to invoke an intermediate state between the equilibrium position of NO on the surface and the gas phase free rotor. If we tried to visualise desorption we would have to imagine it as a very slow process compared to inelastic scattering, requiring many surface-molecule, low-energy collisions. Finally, the last surface-molecule interaction would release the molecule from a weakly bound, nearly freely rotating state with the result of an isotropic distribution of rotational states. A full theoretical study of this process was also carried by Zare et al. Such model used a classical approach and reproduced quite well the experimental findings described above [59].

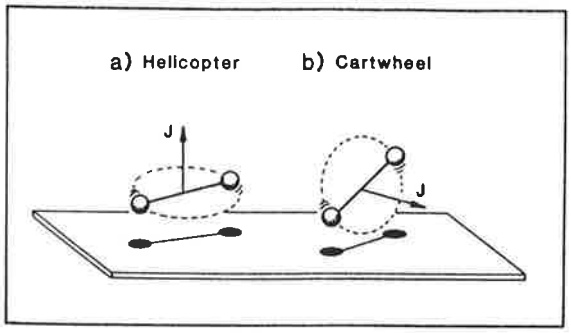

Fig. 14 Schematic diagram of the two most probable orientations of NO on the surface (reprint from ref. 55).

2.1.3 NO / graphite and diamond.

Scattering and desorption experiments have been extended to systems other than transition metal surfaces. Graphite and diamond are just illustrative examples of this new trend in the field. As this section will show, these two surfaces are well suited for both inelastic scattering and trapping/desorption [60].

The experimental set-up required for these surfaces is analogous to those encountered for other familiar systems. A molecular beam is used to select the energy of the incoming molecules. A laser tuned at 226 nm detects the nascents in specific rovibrational states and a cw tunable spin-flip Raman laser is used to generate excited molecules in well defined rovibrational states (i.e. $\upsilon'=1$). This new feature allows a comparison of the internal distribution of products coming from vibrational ground state or excited molecules. Until these experiments were done in the late eighties little was known about the role of vibrational excitation of incoming molecules on the molecule-surface encounter [61-62].

The graphite surface behaves in many ways like most of the transition metal surfaces. At low incident beam energies both trapping and desorption show similar behaviour characterised by the accommodation of the rotational temperature to the surface temperature at low surface temperatures and an enhanced rotational cooling as the surface temperature was raised, indicative of rotational to translational energy transfer for desorption. The only significant difference from other systems was the long residence time of NO on the surface characterised by a very narrow cosine distribution of the desorbing molecules suggesting that a multicollisional process might be a better description than a trapping/desorption mechanism [63].

High beam energies gave rise to inelastic scattering. Rotational populations were characterised by the appearance of rotational rainbows, which suggested an anisotropic rotational momenta. Neither the kinetic energy of the incoming beam nor the vibrational excitation affected these distributions. The hard-cube model was used to explain the observed trends characterised by no significant intramolecular rotational to translational energy transfer and by energy transfer of vibrations to the heat bath, results consistent with the NO/Ag(111) system.

A new approach has been used by Häger and coworkers recently [64]. It involved the use of rotationally-excited molecules for the scattering of NO molecules from a graphite surface. Interestingly enough, they have found that the rotational temperature of the incoming molecules had no influence on the ratio between diffusively (trapping/desorption) and specularly scattered particles. Only the incident kinetic energy and the surface temperature determined the rotational distribution of the products. This means that even for the direct inelastic channel the surface is capable of cooling the rotational degree of freedom so that the molecule loses 'its memory' after impinging the surface. Therefore, a pure translational-rotational energy transfer is not enough to explain the observed results since it is now evident that the surface tries to bring the rotational temperature close to its own temperature. Surprisingly enough, this sort of experiment has been done only in the last one or two years. Nevertheless, in cases like graphite they challenge the currently-accepted mechanisms for inelastic scattering and desorption. What it seems clear now is that the study of the internal energy distribution of the products can only supply us with a partial picture of the overall process. The problem needs to be analysed from the reactant side as well.

Diamond (111) is a very interesting case in itself [60]. Corrugation of the surface is not smeared out by thermal motion at normal temperatures because of its high Debye temperature (2000 °K). This surface has a sawtooth profile so that two different sets of experiments at different surface geometries are required (fig. 15). In scattering experiments similar to those described above, two components for each geometry were discernible.

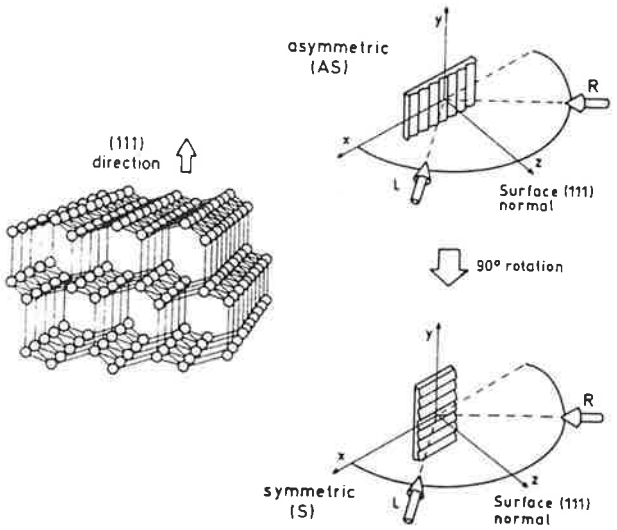

Fig. 15 Diamond (111) surface. Note its asymmetric structure which requires two different experimental geometries (reprint from ref. 65).

The slow component in the TOF spectra had a long residence lifetime on the surface, independent of T_S, which could not correspond to a normal trapping/desorption process. This was explained in terms of the NO molecules trapped in the entrance of the channels on the surface and undergoing many collisions with its walls, the energy transfer determined by the channel direction with respect to the surface. The fast component, however, showed the behaviour characteristic of single or multiple hard collisions with a stiff surface undergoing only rotational to translational energy transfer [65]. After this experiment, two main conclusions were reached for the scattering from hard, corrugated surfaces like diamond (111). First, it was the importance of the specific surface topography on scattering and second the long, temperature-independent residence time on the surface also consequence of the specific geometry of the hard surface.

This overall picture has been modified after the study of the diamond (110) surface [66]. No surface topography dependence was found for this surface even though it has the same basic features as its (111) analogue -i.e. the (110) surface has a pronounced linear symmetric groove structure which is well defined even at high surface temperatures (see fig. 16).

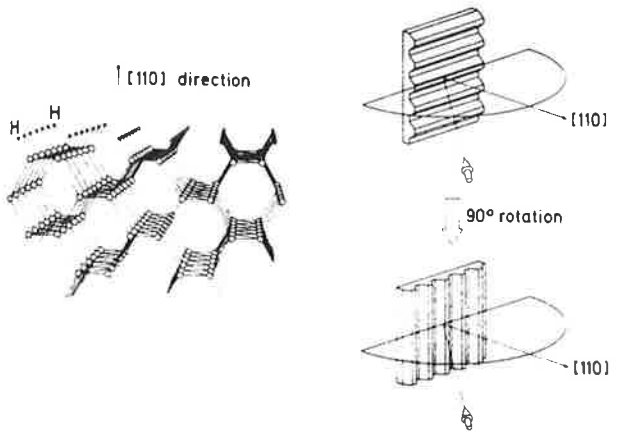

Fig. 16 Diamond (110) surface saturated with hydrogen atoms. Analogous to the other diamond surface, diamond (111), two distinct surface geometries are discernible (reprint from ref. 66).

The experiment showed a transition from a strong translational-rotational coupling at high impact energies to coupling between the surface and molecular degrees of freedom at moderate incoming kinetic energies. The same was observed for vibrationally-excited products. The percentage of vibrational excitation was found to be large and increased with surface temperature in agreement with other systems such as the NO/Ag(111) [62]. Current explanations involve the smoothing of the interacting surface by hydrogen atoms which saturate the dangling carbon bonds. These hydrogens make the surface topography quite uniform so that the same features are obtained regardless of the geometry of the experiment. However, it should be noted that the same saturation effect is common in diamond (111) surfaces yet a clear topographic dependence of scattering has been observed for this system. It remains unclear why one surface, namely the (110), suffers from such effect while the other does not.

2.2 Recombinative desorption.

2.2.1 H_2, D_2 , HD / Cu(110) & Cu(111).

The desorption of hydrogen molecules and isotopic analogues involves a further level of complication compared to simple desorption since a chemical bond is formed during the process. The first studies on recombinative desorption were carried out by Zare and coworkers on the Cu(110) and Cu(111) surfaces in the early eighties [68-70]. This work has been already subject of previous review articles [27] so we will only cite the most significant features related to more novel systems. The rotational distributions were similar for hydrogen and its analogues D_2 and HD, all with a markedly non-Boltzmann character. The vibrational population ratio was found to be surface-structure dependent, and 50-90 times greater than that corresponding to the surface temperature. The mechanism of desorption was thought to involve the formation of a H_2^- anion intermediate.

2.2.2 H_2, D_2 , HD / Pd(100)

Zacharias et al. moved to the Pd(100) system and found that the rotational distributions were also highly non-Boltzmann in agreement with Zare et al. [71]. The same basic experiment has been repeated recently by the same group but this time paying close attention to the vibrationally-excited desorbate in the D_2/Pd(100) system [72]. The amount of vibrational excitation found was nine times larger than expected for molecules at thermal equilibrium with the surface. This vibrational excitation showed an exponential dependence on surface temperature as figure 17 shows below.

Fig. 17 Arrhenius plot of the relative population of vibrationally excited molecules versus the inverse of the surface temperature. Such plot allows to determine how much extra energy needs to be given to the vibrationally-excited desorbing molecules (reprint from ref. 72).

The plot in figure 17 can be analysed using an Arrhenius-type equation. The activation energy was 210±60 mev, which means that it takes more energy to desorb vibrationally excited molecules than ground state ones. The models available to explain recombinative desorption of hydrogen could not explain these findings [73]. Figure 18 shows a schematic diagram of what is currently suggested as the mechanism of hydrogen from palladium.

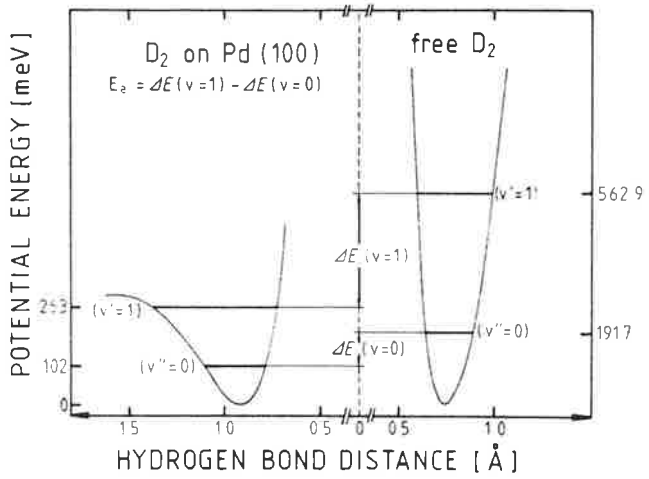

Fig. 18 Potential energy surface of D_2 in the gas phase (left) and on palladium (right). Notice the anharmonicity of the latter and the larger activation energy for molecules in the first excited vibrational state (reprint from ref. 72).

According to this new model, the vibrational levels of the weakly adsorbed D_2 prior to dissociation are very anharmonic compared to those of the gas phase species. The energy barrier that molecules in $\upsilon'=1$ have to surmount in order to desorb is larger than that of the lowest vibrational level. The energy of activation of 210±60 mev obtained from the Arrhenius plot represents the difference between these two energy gaps. This hypothesis is qualitatively supported by recent calculations on the hydrogen-Pt(111) system [74]. This new model assumes that vibrational energy is not transferred to other molecular or surface degrees of freedom. Up to date this assumption has not been tested and even though the model seems plausible, strictly speaking it still remains speculative.

The same results have been obtained for hydrogen and deuterated hydrogen molecules [75]. Prominent rotational cooling was characteristic for H_2, D_2 and also HD. For H_2 and D_2 , the ortho- para- populations were found to be populated statistically. Again, a large proportion of the desorbate was vibrationally excited, the amount of excitation proportional to the surface temperature. Velocity distributions were described by the surface temperature and were totally independent of the rovibrational state probed.

The interpretation of these results becomes difficult due to the absence of realistic potential energy surfaces for this specific system. It seems plausible that only the shape of

this potential energy surface should cause the observed vibrational excitation. Hydrogen desorption can then be understood in terms of shallow potential well where temporary trapping is possible.

Several theoretical models have been used to reproduce the rotational cooling effect [76]. Rotational cooling has been attributed to the rotational to translational energy transfer from the rotating but still adsorbed molecules. Hydrogen molecules reproduced quite well the experimental data but for deuterium theory clearly underestimates rotational cooling (fig. 19).

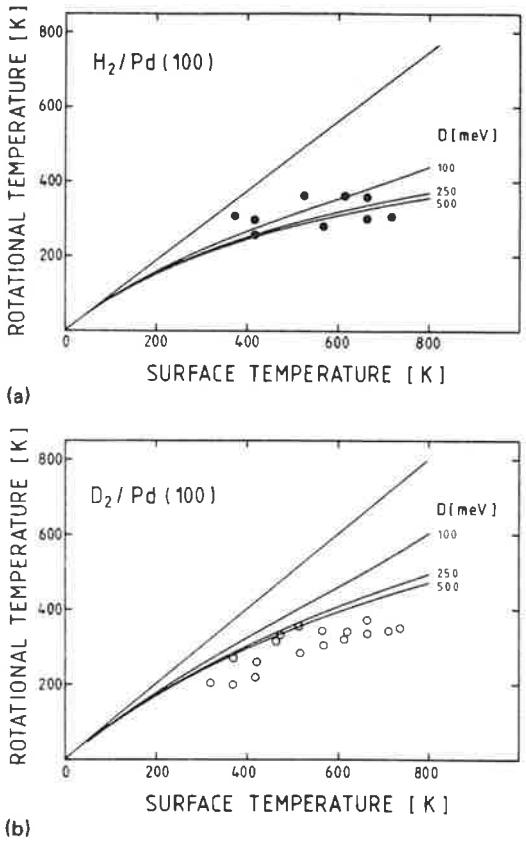

Fig. 19 Experimental rotational temperatures at different surface temperatures plotted against theoretical predictions. Disagreement is clear for the D_2/Pd system (reprint from ref. 75).

However, it should be noted that in the fits shown in figure 19, the rotational constants used are from the gas phase and it assumes that the adsorbed atoms are not affected at all by interactions with electrons in the metal substrate. Thus, conclusive results cannot be obtained from such an oversimplified model. We will have to wait until accurate potential energy surfaces are available for this system to draw any meaningful conclusions.

The study of the hydrogen/palladium system has been taken further in the last two years with special emphasis on the role of coadsorbates. Schröter et al. [77,78] have examined this effect in greater detail. This time, they looked at the change in the

translational and internal energy distributions for specific rovibrational states at different sulphur coverages. For clean palladium, the translational energy was perfectly defined by a Maxwell-Boltzmann distribution for all internal states, isotopomers and surface temperatures. The kinetic energy of the desorbate was linearly proportional to the surface temperature. Interesting changes were found in the internal state distributions. At low sulphur coverage, the rotational temperature was decreased significantly. At high sulphur coverages, the rotational temperature showed the opposite trend. Sulphur coverage also enhanced vibrational excitation. As the sulphur coverage was increased, strong deviations from this type of distribution were found with a velocity independent of the surface temperature. This strongly suggested the appearance a sulphur-induced barrier located in the reaction coordinate before the molecules are formed. If such barrier occurred after recombination then a chemisorption well would be present. However, this chemisorption well has not been observed, consistent with a desorption mechanism that proceeds through a shallow potential well as it has been explained above.

Other changes induced by the presence of sulphur still remain speculative. For example, the change in rotational temperature with sulphur coverage mentioned above can be explained in terms of the adsorption of sulphur atoms on step sites on the surface. At low sulphur coverages, desorption can be approximated by desorption from terrrace sites. At high sulphur coverages creates more defect sites. Rotational excitation is highly dependent on the interaction of the molecule with the anisotropic potential energy surface. Again, this is nothing but speculation and full theoretical treatment of the problem needs to be addressed before a fruitful interpretation of the experimental data can be reached.

2.2.3 H_2, D_2 , HD / Si(100)

Very few publications are currently available in the literature for the hydrogen-silicon system. Only after the work performed on copper and palladium surfaces it has been possible to examine non-metal surfaces. Pioneers in this area are the group led by Richard N. Zare at Stanford University, who has published the first state-resolved studies on hydrogen desorption from silicon surfaces [79,80]. One of the most important factors that have held back the growth in number of these experiments is the need to have, on the one hand a complete characterisation of the surface and on the other hand detailed information on the molecule which is detected state-selectively.

Fortunately, previous work in the gas phase has provided such data for hydrogen [81] and the Si(100) surface has been fully characterised by STM. The state-resolved studies showed that the vibrational population in the υ=1 state was twenty times higher than predicted by a Boltzmann distribution equilibrated with the surface temperature. Rotational populations and the amount of rotational cooling were independent of the isotopic species used indicating tunnelling effects in the desorption mechanisms were unimportant.

Such superthermal vibrational population has also been observed for the hydrogen/copper and hydrogen/palladium systems [68-72]. It is indicative of an elongated equilibrium bond distance compared to the gas phase at the moment of desorption. Since the reaction is endothermic, vibrational excitation can only come from the shape of the potential energy surface.

The rotational cooling was caused, as in many other systems, by rotational-translational energy transfer. Rotational temperatures were usually very low, roughly half of the surface temperature. This implies that little torque is applied to the molecule due to some dynamical constraint in the desorption channel. Calculations on this system show that the lowest energy pathway for desorption is an approach that is not only parallel to the surface but also aligned with the silicon dimer present in the Si(111)2x1 surface (fig. 20).

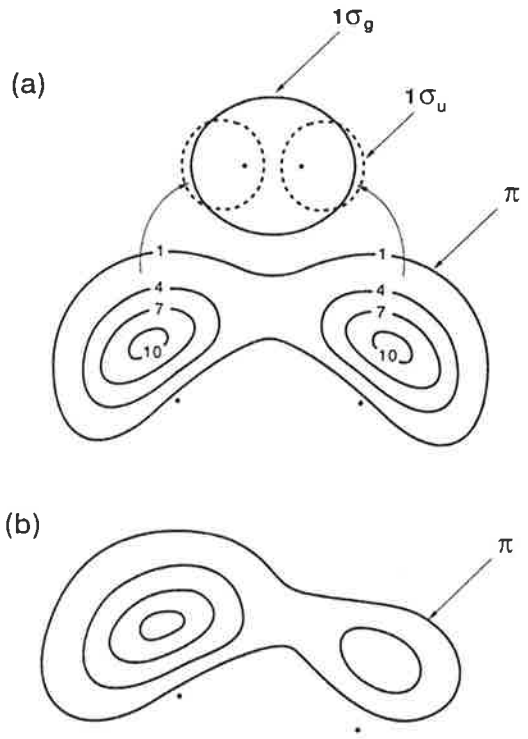

Fig. 20 Schematic diagram of the three-center transition state proposed for H_2 desorbing from Si(111). (a) shows the most important electronic states and electron densities of both hydrogen and the Si-dimer; (b) shows the asymmetric character of such electron distribution when hydrogen is near the surface, in agreement with experimental evidence (reprint from ref. 79).

There is recent evidence [80] that supports the idea of a three-centre transition state in which the hydrogen molecule is more likely to be much closer to one end of the silicon dimer. If this holds true, desorption would start from a paired set of hydrogens adsorbed on a silicon dimer unit. One hydrogen then migrates to the other side of the dimer to initiate concerted desorption passing through a three-centre transition state with an

elongated H-H bond leading to vibrational excitation. The symmetry of hydrogen molecules would ensure that no significant torque is given to the desorbing molecule during desorption.

2.2.4 Other systems: CuF/LiF, As_2/Si(100)

Näher et al. [82-84] have looked at the rotational distribution of CuF molecules associatively desorbing from copper surfaces. Studies of this sort have been estimulated by previous work such as that of Zare et al. [55]. Two distinct rotational distributions, both cooler than the surface temperature indicated either a preference for low J states or two distinct desorption channels. The extent of rotational cooling was found lower compared to the NO or H_2 Pt(111) systems. Rotational alignment was measured in a similar fashion to that already described for NO/Pt(111) in section 2.1.2. A greater component of the J axis of the desorbate was found aligned parallel to the surface normal showing a preference for helicopter motion.

Leone et al. have paid attention to the vibrational distribution of As_2 in the cracking of As_4 on Si surfaces [85,86]. It was found that the desorption yield increased with the surface temperature after a certain level and then decreased dramatically. This was interpreted as a dissociative process controlled by different competing rate processes that dominate in different temperature ranges. For both Si(100) and Si(111), effective vibrational temperatures were 300-400 ^{o}K colder than the surface temperature suggesting some type of non-equilibrium dynamics involved in desorption. Two mechanisms are possible in view of this evidence. It is possible that as the atoms recombine at the surface only one of them remains bound to the surface. Then, the coupling of vibrational energy of the As dimer into the As-Si bond reduces the vibrational excitation. It is also equally plausible that vibrationally cold molecules tend to desorb better since molecules with high vibrational energies would be proned to dissociate again and return to the surface. This, for example has been observed already in the H_2 /Pd(100) system [72,87].

2.3 Laser and electron induced desorption (LID/ESD).

2.3.1 NO/Pt(111).

The NO/Pt(111) system has also been investigated using laser and electron induced desorption (LID and ESD). Cavanagh et al. [17] have studied the laser-induced desorption (LID) of this system. Using LIF and TOF techniques it was possible to characterise the kinetic and internal energy distributions for a wide range of conditions (desorption laser wavelength, fluence, incident angle and polarisation). An analysis of TOF spectra in specific states allowed the determination of rotational, vibrational, spin-orbit and lambda doublet populations.

They found two separate velocity distributions due to two different binding sites, in agreement with previous studies [88]. The internal distributions of the slow component had both rotational and spin-orbit populations at equilibrium. The fast component, however, showed a trend of increasing kinetic energy with rotational quantum number J.

In addition, rotational energy and spin-orbit populations were markedly non-Boltzmann especially below 300 cm^{-1}. Surface coverage did not seem to affect either the kinetic energy or the internal energy, including vibrations. Raising the surface temperature increased the characteristic translational and rotational temperatures but did not change the Boltzmann nature of the distributions.

The data described above was interpreted in terms of two distinct desorption channels. The slow kinetic energy component was consistent with the expectations of LID thermal desorption in the absence of dynamical constraints. For the fast component, the wavelength dependence of the kinetic energy distributions and the lack of correlation of the internal energy with laser wavelength used to induce photodesorption suggested that NO interacts with 'hot carriers'. This excitation mechanism is not a result of interaction with thermalised excitation and involves either excitations in the bulk or direct excitation of the NO-Pt complex. These photogenerated carriers induce desorption via the formation of a temporary ion resonance. Furthemore, the minimum of this excited state being tilted away from the surface normal agrees with the non-Boltzmann spin-orbit distributions found for the fast component. Moreover, such tilted state was found to be consistent with a hot electron interacting with the adsorbate forming a transient anion and excluded the involvement of any localised excitations of the adsorbate-substrate complex.

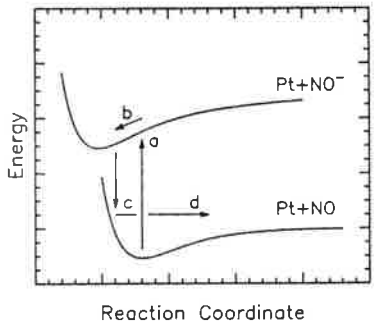

Fig. 21 Simplified picture of the laser-induced desorption mechanism via a temporary ion resonance: in (a) the negative ion is formed by the uptake of a hot electron; the ion evolves on the excited potential energy surface (b) and is finally neutralised (c); neutralisation returns the molecule back to the repulsive part of the ground state potential and desorption occurs (d) (reprint from ref. 17).

These results agree qualitatively with electron-stimulated desorption (ESD) experiments performed on clean and oxygen-covered Pt(111) surfaces [89]. These experiments made use of REMPI/TOF to detect the desorbed NO through the well-known $A^2\Sigma^+(\upsilon')$-$X^2\Pi_{1/2,3/2}(\upsilon'')$ resonance-enhanced (1+1) ionisation band.

ESD thresholds of 9-10 eV were measured for the $\upsilon'=0,1,2$ vibrational levels both on the clean and oxygen-covered surface [89-92]. This threshold was assigned to a hole occupying the non bonding 5σ molecular orbital. $5\sigma^{-1}$ excitation was screened by charge transfer into the $2\pi^a$ molecular level. The narrow character and the increasing dependence of the translational distribution with oxygen coverage (0.13 ev change between θ_o=0.4 and

0.75) was explained as an outcome of the decrease in the $2\pi^a$ screening charge in the presence of oxygen on the surface. This idea is consistent with the decrease in vibrational energy observed for the oxygen-covered surface. The $2\pi^a$ orbital is non bonding and decreasing the metal screening charge into this level should reduce the energy of the aforementioned degree of freedom. The lower rotational energies for the coadsorbed system as well as the increase in translational energy for the (NO+O) system were consistent with this overall picture. Analogous effects have been found in the NO_2 Pd-O system [93].

A new spectroscopic technique devised recently has been used in this system [94]. It consists of a two dimensional imaging method which measures energy and angular distributions of photogenerated or photodesorbed products. Initially, a laser is used to excite the adsorbate-substrate complex. A tunable UV probe laser ionises the desorbate via REMPI. The delay time between the probe and the excitation laser is electronically modified to obtain a sequence of images from which the translational energy distributions at several desorption angles can be deduced. Even though, the results from this experiment agree quite well with previous experiments, the kinetic energy distributions were clearly non-Maxwellian with only a single component in the TOF spectra instead of two and the angular distributions were best fitted to a $\cos^4\alpha$ instead of the previously reported $\cos^{11}\alpha$ dependence [17]. The major conclusion from this experiment was on the one hand the urgent need to revise in full depth this system once again. It seems clear now that no degree of freedom is at equilibrium with the surface and that desorption is induced via electronic excitation. However, it is quite possible that the mechanism mentioned above for the LID of Pt(111) involving photogenerated hot carriers might not be appropriate in light of these new findings.

2.3.2 NO/Pd(111).

Recently, the surface dynamics of NO has been studied on other metal surfaces in an attempt to obtain a less fragmentary picture of the induced desorption mechanisms of this species. E. Hasselbrink et al. [95] have reported fully state-resolved measurements of translational, rotational and vibrational internal energy distributions for NO molecules desorbing after the photodissociation of NO_2 on Pd(111). Experiments were performed with NO_2 adsorbed on top of a saturated layer of chemisorbed NO to avoid strong chemisorption of NO_2 on the surface. TPD showed that NO_2 on the surface was present in its dimer form, N_2O_4.

State-selected TOF data using LIF was used to elucidate the mechanism of photodissociation. From the TOF spectra two different desorption channels were detected: a fast one, with energies above the surface temperature and a slow one fully accommodated to the surface. The use of polarised incident radiation at various incident angles determined that primary photon absorption occurred in the metal and not on N_2O_4. This finding was corroborated by the observed photodissociation cross sections, linearly proportional to the excitation energy of the laser and ten times larger than those found in the gas phase.

Internal distributions were measured in two modes: at a fixed velocity allowing the determination of characteristic rotational and vibrational temperatures and at a fixed

rovibrational state. The slow channel was predominant at low J while the fast one appeared at high J. Only the fast channel showed a linear increase of kinetic energy with internal energy. Single rotational temperatures around 900°K were characteristic of the fast component while the slow showed both cold (140°K) and hot (470°K) contributions. Vibrational populations were difficult to measure but it was estimated that the $\upsilon'=1$ state had an occupancy of a few percent, corresponding to high vibrational temperatures circa 1000°K.

The state-specific data suggested a dissociating electron attachment mechanism. Such a mechanism consists of bond breaking initiated by transient formation of a negative ion resonance. Evidence supporting this hypothesis comes from the known tendency of N_2O_4 to form NO^+ and NO_3^-, NO^+ being the fragment neutralised by the electron. Then the fast channel, markedly non-Boltzmann, would arise from the repulsive part of such potential of interaction and the slow channel could come from thermal accommodation of NO^+ prior to interaction with the electron. This mechanism accounts for observations such as the disappearance of the second reaction product, oxygen, in the course of the experiment.

The dynamics of the fast channel was thought to proceed via excitation of the molecule to a repulsive excited state (i.e. negative ion resonance) which will cause energy redistribution into all degrees of freedom, including the dissociation coordinate. In the case of rapid quenching of this excited state by the metal, the amount of excitation will be determined by the residence time in the excited state. If such lifetime is long enough, quenching of the excited state by the metal will generate a ground state molecule with unfavourable geometry that might fall apart releasing NO. This process is consistent not only with the vibrational and rotational excitation but also with the positive linear correlation between kinetic, vibrational and rotational energies. This same model, for example, has been used to explain the electron-stimulated desorption of NO on Pt(111) [90]. It is premature to extrapolate all the conclusions found for both Pt(111) and Pd(111) to other systems. Nevertheless, it shows that there are some common mechanisms for the desorption of NO from different surfaces.

Up until now all experiments have been restricted to desorption using excitation sources of at least nanosecond duration or longer. In the last couple of years it has been possible to study desorption using femtosecond laser pulses. The time resolution of these experiments is comparable to the duration of energy flow which occurs in the picosecond and femtosecond time scale. In these experiments, strong non-equilibrium conditions can be attained and the mechanisms observed are impossible to explain in any conventional way.

Prybyla et al. [97] have used 200 fs pulses at 620 nm and a REMPI/TOF detection scheme to investigate the desorption of NO from a Pd(111) surface. The first manifestation of non linearity was found in the behaviour of the desorption yield with laser fluence. Figure 22 shows this dependence, fitted to a polynomial of order 3.3.

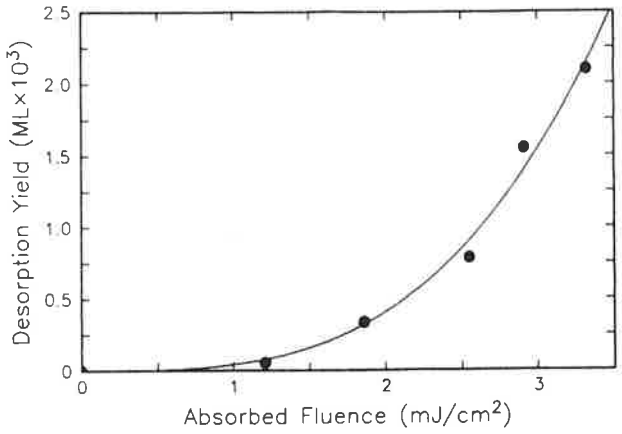

Fig. 22 Desorption yield of NO as a function of adsorbed laser fluence (reprint from ref. 97).

Translational energy distributions obeyed a Maxwellian distribution and were independent of the internal quantum state. From the internal-state distribution analysis it became apparent there was a high degree of vibrational excitation (T_{vib}=2200°K). In addition, rotational distributions were markedly non-Boltzmann and the spin-orbit temperature was unusually high (see fig. 23).

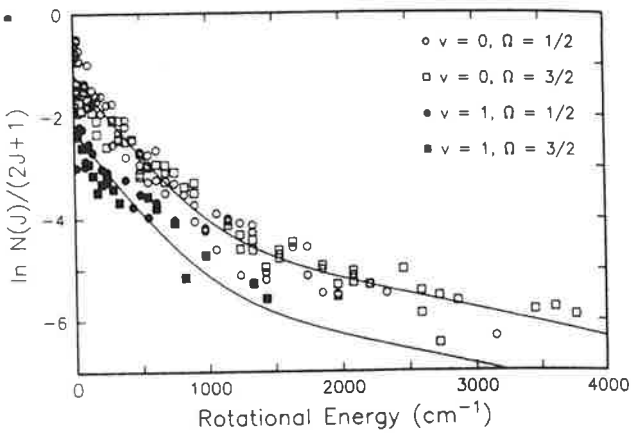

Fig. 23 Rotational state distribution of desorbed NO for the $\upsilon''=0,1$ $A^2\Sigma^+(\upsilon')$-$X^2\Pi_{1/2,3/2}$ bands (reprint ref. 97).

Neither the desorption rate nor the internal state populations, especially the high vibrational temperature, could be explained using a known model of desorption. Clearly, the femtosecond regime offers a new range of desorption dynamics never observed before. The model proposed invokes a desorption mechanism via an excited electronic state,

compatible with the energy distribution (i.e. high vibrational energy is due to changes in bond length after the photoinduced transition). The large cross sections or desorption rates were attributed to either an enhanced flow of energetic electrons at the surface or to multiple excitation of adsorbed NO molecules.

Current progress in femtosecond desorption include time-resolved measurements of NO desorbing from Pd(111) [98]. These studies make use of a two-pulse correlation scheme. Desorption yields are measured as a function of temporal separation between excitation pulses. A lifetime of 1 picosecond (ps) has been assigned to the excitation responsible for desorption. Thermal desorption processes are ruled out due to their long lifetimes (about 10 ps) showing the inadequacy of treating desorption as an instantaneous process at least in this time regime. This time-resolved technique was combined with REMPI to study the $\upsilon''=0$ and Q+P bandheads.

Evaluation of the lifetimes for different desorption mechanisms allowed to assess the importance of electronic excitation in the substrate as responsible for desorption. The experimental features observed can only be explained by considering the electronic temperature in the metal substrate not the lattice temperature, demonstrating the importance of low-energy electronic excitation in coupling substrate energy to the motion of the adsorbate on the metal surface. Even though previous studies had hinted at this before, the advent of femtosecond desorption experiments has provided the ultimate tool for the evaluation of the most important dissociation mechanism.

2.3.3 NO/Pt(001).

The photo-induced desorption mechanism of NO on this surface can be explained by invoking some of the most common mechanisms already introduced for very well studied systems such as NO/Pt(111) and NO/Pd(111).

Kazuhiro Mase et al. [99-101] have noticed that the photodesorption yield increased drastically when the exposure was equal to or greater than 1.8 L, suggesting that the NO responsible for the desorption channel increased drastically in concentration after this surface coverage. Three adsorption sites have been characterised for the NO/Pt(001) system. However, only one, namely the adsorbed on-top state in Pt(20x5), is present at high coverages. This finding agrees with experiments performed by Buntin at al. on Pt(111) where it was found that only the on-top site was sensitive to photodesorption [102]. The on-top site is weakly chemisorbed with respect to others and can be photodesorbed easily.

The NO^+ yield was found to be linearly proportional to laser fluence for both s and p linearly polarised light, indicative of a one-photon process. However, p-polarised light had desorption yields three times larger than s-polarised radiation. Internal state distributions and translational energies were independent of the polarisation of the pump laser. In view of the fact that s- and p- polarised light are able to induce desorption, two mechanisms are plausible: direct valence-electron excitation in the NO-Pt complex; or electronic excitations in the platinum substrate followed by electron transfer of hot electrons into an unoccupied orbital of chemisorbed NO.

These two types of mechanism have been used to explain the dynamics of desorption for both the Pt(111) and Pd(111) systems [17]. According to the model proposed

by Burns et al. [90], NO is desorbed via an almost neutral state with a screened 5σ hole. The mechanism consists of a 5σ to $2\pi^a$ transition followed by resonant tunnelling of $2\pi^a$ electrons into the Pt conduction band. The 5σ hole has a long lifetime that allows the adsorbate molecule to acquire sufficient energy to escape from the surface. The kinetic and internal distributions measured for this system agree with those predicted by the model. In the mechanism suggested by Buntin et al. [17], NO desorbs via a negative ion resonance excited state created by electron transfer from hot electrons photogenerated in the substrate and transferred into the $2\pi^a$ orbital of the NO-Pt complex. However, the predictions of this mechanism on the internal energy partitioning do not agree with the experimental data.

As we have seen in this section, internal state analysis becomes the ultimate tool to determine the best mechanism of a surface-mediated process. Fortunately, the Pt(001) surface is quite similar to Pt(111) and that allows an almost complete extrapolation of results from one to the other. However it should be borne in mind that this practice becomes dangerous when the substrate or adsorbate are of a markedly different nature.

2.3.4 NO/Si(111).

The laser-induced desorption on semiconductor surfaces has been investigated recently partly because of the technological implications that it entails but mainly because it has been possible to develop a fairly complete picture of all possible mechanisms of induced desorption on well-characterised metal surfaces.

Richter et al. [105] have studied the LID of NO from Si(111) paying particular attention to the effects of coverage on NO vibrational populations. They used both B-doped p-type and P-doped n-type substrates and several laser desorption wavelengths ranging from 355 to 1907 nm. Quantum-state resolution was achieved with a LIF/TOF setup which allowed the determination of vibrational, spin-orbit and rotational populations.

The internal state distributions were found to be extremely sensitive to coverage. At low coverages the rotational populations could be described by a single rotational temperature independent of vibrational excitations but clearly biased to occupy the F_1 spin-orbit state. At saturation coverage, the rotational population had a higher rotational temperature coincident with the spin-orbit one. The remarkable difference was the relative ratio of vibrationally-excited molecules at each coverage: at low coverages, 20% in the $\upsilon'=1$ state and 0.04% in the $\upsilon'=2$; at saturation coverages, 57% and 10% respectively. Also important to note is the dependence of the yield with laser fluence, linear at low coverages (i.e. one-photon excitation) but sublinear at high coverages.

The stark differences between both coverages were indicative of two different mechanisms of desorption. The coverage dependence arises from the quenching of the low coverage mechanism by the appearance of the high coverage one. Three possible mechanisms are possible: first, direct neutralisation of the charged adsorbate in the ground state, leading to desorption of the neutral species on a repulsive potential energy surface (PES); second, formation of a negative ion resonance of the adsorbate, leading to motion on an excited PES and finally desorbing after ion neutralisation, a model proposed by Weeks et al. [103]; third, recombination enhanced diffusion where localised lattice

excitations created during carrier recombination result in a nonthermal reaction. Considering just the vibrational state populations, the three models are equally likely.

An intensive investigation of the saturation coverage regime has been done by Ying at al. [104]. The LID under these conditions was attributed to the interaction with hot carriers; such a mechanism was supported by the observation that the wavelength dependence of the yield was reproduced by a simple expression derived from a model involving only hot carriers produced at the surface.

Richter et al. have continued the study of the Si(111)7x7 surface focusing on the low coverage mechanism [105]. Fig. 24 below shows a plot of the LIF signal versus the NO exposure; three areas are clearly discernible: a low coverage, a transition and a high coverage region. Focus on the low coverage region showed that the kinetic energy of the products was proportional to the rotational number probed with a preference for the F_1 spin-orbit state as observed before but with no difference between molecules in the different vibrational states.

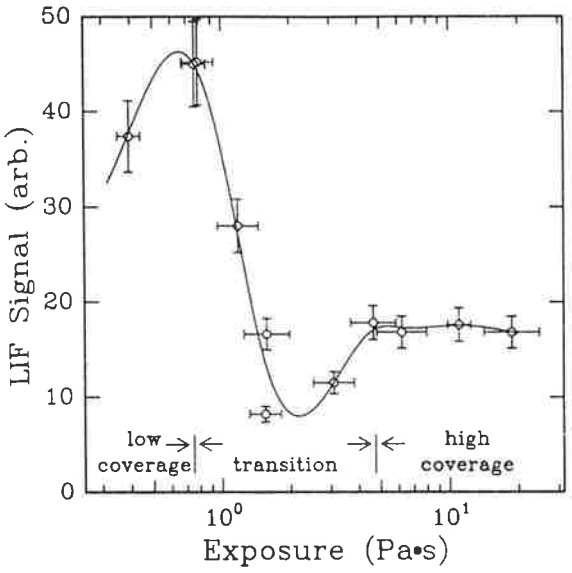

Fig. 24 LIF intensity as a function of coverage. The areas are clearly discernable, consistent with two different desorption regimes at high and low coverages (reprint from ref. 105).

Desorption was clearly peaked along the surface normal, indicative of a highly anisotropic mechanism. Even more interesting was the coupling between the vibrational degree of freedom and the laser desorption wavelength. Vibrational excitation became negligible for wavelengths larger than 1064 nm, reflecting energy constraints in the desorption mechanism. The only mechanism consistent with these findings was a surface-localised excitation involving the creation of a hole in the normally occupied S_2 surface state band which is quenched at higher coverages by NO. This surface-state excitation is able to induce the observed surface chemistry. These surface states depend on both

structure and adsorbate traits. Thus, surface-state driven reactions are potentially anisotropic and might be usefully controlled by appropriate coadsorbates which activate specific surface states. This leads to the highly attractive idea of engineering photoreactions by the proper choice of adsorbate, coadsorbate and surface.

The details of the NO desorption mechanism from Si(111)7x7 remain highly speculative. It would be necessary to contrast the experimental results against a full theoretical treatment of this system which is not available yet. Certainly, desorption must be faster than the vibrational relaxation lifetimes since vibrations are decoupled from other degrees of freedom. This is supported by the faint memory of the photon energy in the NO energy content. The energy coupling between rotation and translation is indicative of desorption from a repulsive excited state. This is consistent with a charge transfer from an adatom-bound $NO^{-\delta}$ adsorbate to the S_2 hole localised on a rest atom, projecting the NO onto an excited PES that results in prompt desorption.

2.3.5 Other systems: CO/Ni(111), CH_3I/MgO.

Assher et al. [30] have studied the photodesorption of CO from Ni(111)-O surface using LIF. In contrast with the NO/Pt system [17], TOF spectra was not affected by laser fluence and had no bimodal velocity distribution. Furthermore, a single rotational temperature could not describe the results and the rotational distributions were also unaffected by varying the energy of the excitation laser. The same rotational distributions were found for vibrationally excited states. Finally, the amount of vibrational excitation was considerable, the vibrational temperature reaching values of 1400°K. It seems clear that desorption was not thermally activated due to the large amount of vibrational excitation and the decoupling of translational and rotational distributions with respect to the fluence of the excitation source. Two mechanisms are possible: the breaking of the adsorbate-substrate bond due to direct excitation or a substrate-mediated process such a 'hot carrier' mechanism which would lead to high translational and vibrational excitation due to the long residence lifetime of the excited intermediate state. Moreover, the existence of two different rotational distributions might be indicative of two different CO photoactive species on the surface.

The photodissociation of methyl iodide on MgO with 257 nm pulses is probably one of the most complex systems found in the recent literature [67]. The photodissociation of methyl iodide in the gas phase is quite well understood [96]. Considering the ratio of I and I* (excited) products from dissociation one finds that on the surface less I* species is formed. Evidence of photoinduced surface reaction in addition to photodissociation was found in the non-resonant signals in the REMPI spectra corresponding to I_2^+ and I^+ which required the absorption of two photons, suggesting a mechanism involving the photoproduction and removal of an intermediate species which originates from a chemical process involving iodine trapped at the surface, preferentially I*.

3. Conclusions.

State-selective techniques have undoubtedly increased our understanding of the basic mechanisms of dynamical processes occurring on surfaces. In very broad terms, molecule-surface interactions fall into two categories: direct-inelastic scattering and trapping/desorption. In the first case, a molecule striking the surface undergoes only incomplete exchange of translational energy with the solid, the interaction is of single collision type and the population of rotational levels of the scattered particles is primarily governed by translational-rotational energy transfer mediated by the solid surface which normally leads to rotational cooling. The second case involves complete accommodation of the initial translational energy to the surface, where the molecule spends a longer, measurable lifetime at the bottom of the attractive well before it is released back into the gas phase through coupling of its various degrees of freedom to the heat bath of the solid. Obviously, these two cases represent the two extremes of a broad spectrum of molecule-surface processes.

A very different approach has used non-thermal means of excitation such as lasers or electrons. Lasers, for example, are able to induce non-thermal processes which cannot be adequately explained by adsorbate interactions with a lattice bath even at very high temperatures. The very intense radiation generated by these light sources can create excitations of the electronic states in the adsorbate, adsorbate-substrate complex or substrate and induce highly specific chemistry on the surface. The use of state-selective spectroscopic techniques has played a crucial role in this area. As illustrated in section 2.3, several mechanisms of excitation have been proposed. These could be classified into two categories: direct and indirect. Direct mechanisms involve either an optical excitation of the adsorbate or of the adsorption complex. On experimental grounds, direct mechanisms are distinguished by whether the initial excitation is a transition between states similar to localised states of the free molecule or between states arising from the presence of the chemisorption bond. In general, indirect mechanisms can be also of two types, namely substrate-mediated photochemistry or photoinduced thermal chemistry. The former, for example, will occur if the electronic excitation migrates to the surface and efficiently couples to the reaction coordinate before it is degraded to heat. Interestingly enough, each mechanism is characterised by specific internal and translational energies of the desorbate and on other experimental data such as reaction cross sections and the dependence of the yield on laser fluence. In very rare cases it has been possible to discern between these mechanisms without invoking state-specific data.

As of today, and despite the large amount of literature on the subject, scientific knowledge in this area is far from being complete. Only nitrogen oxide and hydrogen interacting with a reduced number of surfaces have a more or less complete picture. The main obstacle is the need to have very detailed information not only about the surface of interest but also about the molecule scattering or desorbing from it. Unfortunately, this restricts the field to very few other simple systems (i.e. carbon monoxide, methyl iodide, etc). Clearly, this is just the beginning of a very long road that leads to a complete understanding of the dynamics of chemical reactions on surfaces.

4. Acknowledgements.

My most sincere thanks to my supervisor Dr. D. O. Hayward for his patience while leading me through the vast literature and correcting the various drafts of this paper.

I would also like to thank Dr. Angel Gonzalez Urena from the Universidad Complutense de Madrid for providing me with very useful material on the basic aspects of laser spectroscopy.

5. Bibliography

[1] Schultz, A., Cruse, H. W., Zare R. N., *J. Chem. Phys.* **57**, 1972: 1354-55
[2] Sinha, M.P., Schultz, A., Zare, R. N., 1973. *J. Chem. Phys.* **58**, 1973: 549-56
[3] Zare, R. N. , Dagdigian, P.J., *Science* **185**, 1974: 739-47
[4] Frenkel, F., Campbell, C.T. et al., *Phys. Rev. Lett.* **46**, 1981: 152
[5] McClelland, G. M., Kubiak, G. D., Rennagel, H. G., Zare, R. N., *Phys. Rev. Lett.* **46**, 1981: 831
[6] Kleyn, A. W., Luntz, A. C., Auerbach, D. J., *Phys. Rev. Lett.* **47**, 1981: 1169
[7] Thorman, R. P., Bernasek, S. L., *J. Chem. Phys.* **74**, 1981: 6498
[8] V. S. Letokhov et al. 'Laser Analytical Spectrochemistry', Adam Hilger, Bristol and Boston, 1986
[9] R. N. Zare, *Far. Disc. Chem. Soc.* **67**, 1979: 7
[10] David R. Crosley, *J. Chem Ed.* **59**, 1982: 446
[11] Zewail, A. H., 'Laser Chemistry', *Physics Today* **33**, 1980: 43
[12] Breit, G., *Rev. Mod. Phys.* **5**, 1933: 91-140
[13] James L. Kinsey, *Ann. Rev. Phys. Chem.* **28**, 1977: 349
[14] R. D. Levine and R. B. Berstein: 'Molecular Reaction Dynamics and Chemical Reactivity'. Oxford University Press. 1987
[15] Greene, C. H., Zare, R.N., *J. Chem. Phys.* **78**, 1983: 6741-53
[16] Altkorn, R. and Zare, R. N., *Ann. Rev. Phys. Chem.* **35**, 1984: 265-89
[17] S. A. Buntin, L. J. Richter, D.S. King, R. R. Cavanagh, *J. Chem. Phys.* **91**, 1989: 6429
[18] V.S. Letokhov, 'Laser Analytical Spectrochemistry', The Adam Hilger Series on Optics and Electronics, Adam Higer, Boston,1986
[19] Hollas, J.M., 'Modern Spectroscopy', John Wiley and Sons, New York, 1992: section 9.3
[20] D.L. Andrews, 'Lasers in Chemistry', Springer-Verlag, 1986: 129
[21] V. S. Letokhov, 'Laser Photoionization Spectroscopy', Academic Press, New York, 1987
[22] Johnson, P.M. and Otis, C.H., *Ann. Rev. Phys. Chem.*, 1981: 139
[23] King, D.S. and Cavanagh R.R., 'Laser Surface Studies '(Springer, Berlin, 1984)
[24] Kubiak, G.D., Sitz, G.O. and Zare R.N., *J. Chem. Phys.* **83**, 1985: 2538
[25] Jacobs, D.C. and R.N. Zare, *J. Chem. Phys.* **85**, 1986: 5457
[26] Jacobs, D.C., Madix, R.J. and R.N. Zare, *J. Chem. Phys.* **85**, 1986: 5469
[27] M. C. Lin and G. Ertl, *Ann. Rev. Phys. Chem.* **37**, 1986: 587-615
[28] Barker, J. A., Auerbach, D. J., *Surf. Sci. Rep.* **4**, 1985:1

[29] Zacharias, H., *Applied Phys.* **A47**, 1988: 37
[30] M. Assher, F. M. Fimmermann, L. L. Springsteen, P. L. Houston, *J. Chem. Phys.* **96**, 1992: 4808
[31] R. R. Cavanagh, S. A. Buntin, L. J. Richter, D. S. King, *Comments At. Mol. Phys.* **24(6)**, 1990: 365-376
[32] Barker, J. A., Auerbach, D. J., *Surf. Sci. Rep.* **3**, 1985: 413-95
[33] McClelland, G. M., Kubiak, G. D., Rennagel, H. G., Zare, R. N., *Phys. Rev. Lett.* **46**, 1981: 831-4
[34] Kubiak, G. D., Hurst, J. E. Jr., Rennagel, H. G., McClelland, G. M., Zare, R. N., *J. Chem. Phys.* **79**, 1983: 5163-78
[35] A. W. Kleyn, A. C. Luntz, and D. J. Auerbach, *Phys. Rev. Lett.* **47**, 1981: 1169
[36] A. C. Luntz, A. W. Kleyn, and D. J. Auerbach, *J. Chem. Phys.* **76**, 1982: 737
[37] A. C. Luntz, A. W. Kleyn, and D. J. Auerbach, *Phys. Rev. B* **25**, 1982: 4273
[38] A. C. Luntz, A. W. Kleyn, and D. J. Auerbach, *Surf. Sci.* **117**, 1982: 33
[39] A. C. Luntz, A. W. Kleyn, and D. J. Auerbach, *Surf. Sci.* **152**, 1985: 99
[40] J. Misewich and M. M. T. Loy, *J. Chem. Phys.* **84**, 1986: 1939
[41] Nichols, W. L., Weare, J. H., *J. Chem. Phys.* **62**, 1975: 3754
[42] Rettner, C. T., Fabre, F., Kimman, J., Auerbach, D. J., *Phys. Rev. Lett.* **55**, 1985: 1904
[43] Muhlhausen, C. W., Williams, L. R., Tully, J. C., *J. Chem. Phys.* **83**, 1985: 2594
[44] C. T. Rettner, J. Kimman, and D. J. Auerbach, *J. Chem. Phys.* **94**, 1991: 734
[45] C. T. Rettner, *Vacuum* **38**, 1988: 295
[46] G. O. Sitz, Andrew C. Kummel, and R. N. Zare, *J. Chem. Phys.* **89**, 1988: 2588
[47] H. Vogues, and R. Schinke, *Chem. Phys. Lett.* **100**, 1983: 245
[48] M. G. Tenner, F. H. Geuzebroek, et al., *Chem. Phys. Lett.* **168**, 1990: 45
[49] F. Frenkel, J. Häger, W. Krieger, H. Walther, C.T. Campbell, G. Ertl, H. Kuipers, and J. Segner, *Phys. Rev. Lett.* **46**, 1981: 152
[50] J. Segner, H. Robota, W. Wielhaber, G. Ertl, F. Frenkel, J. Häger, W. Krieger, and H. Walther, *Surf. Sci.* **131**, 1983: 273
[51] M. Assher, W. L. Guthrie, T.-H Lin, and G. A. Somorjai, *Phys. Rev. Lett.* **49**, 1982: 76
[52] M. Assher, W. L. Guthrie, T.-H Lin, and G. A. Somorjai, *J. Chem. Phys.* **78**, 1983: 6992
[53] D. C. Jacobs, K. W. Kolasinski, R. J. Madix, and R. N. Zare, *J. Chem. Phys.* **87**, 1987: 5038
[54] D. A. Mantell, R.R. Cavanagh, D. S. King, *J. Chem. Phys.* **84**, 1986: 5131
[55] D. C. Jacobs, K. W. Kolasinski, S. F. Shane, and R. N. Zare, *J. Chem. Phys.* **91**, 1989: 3182
[56] A. R. Burns, E. B. Stechel, and D. R. Dennison, *Phys. Rev. Lett.* **58**, 1987: 250
[57] M. E. Bartram, B. E. Koel, and E. A. Carter, *Surf. Sci.* **219**, 1989: 467
[58] D. A. Mantell, R.R. Cavanagh, D. S. King, *J. Chem. Phys.* **82**, 1985: 1046
[59] D. C. Jacobs, and R. N. Zare, *J. Chem. Phys.* **91**, 1989: 3196
[60] Häger J., Walther H., *Annu. Rev. Mater. Sci.* **19**, 1989: 269-93
[61] Rettner, C. T., Fabre, F., Kimman, J., Auerbach, D. J., *Phys. Rev. Lett.* **55**, 1985: 1904
[62] Kimman, J., Rettner, C. T., Fabre, F., Auerbach, D. J., Morawitz, H., *Surf. Sci.* **192**, 1987: 107
[63] Vach, H., Häger J., and Walther H., *J. Chem. Phys.* **90**, 1989: 6701

[64] Häger. J., Roth, M., Walther, H., *Chem. Phys. Lett.* **189**, 4-5: 420
[65] Matsuo, Y. et al., *J. Chem. Phys.* **93**, 1990: 4368
[66] Roth, C., Häger J., and Walther H., *J. Chem. Phys.* **97,** 1992: 6880
[67] K. A. Trentelman, D. H. Fairbrother, P. G. Strupp, P. C. Stair, and Eric Weitz, *J. Chem. Phys.* **96**, 1992: 9221
[68] Kubiak, G. D., Sitz, G. O., Zare R. N. *J. Chem. Phys.* **81,** 1984: 6397
[69] Kubiak, G. D., Sitz, G. O., Zare R. N. *J. Vac. Sci. Technol.* **A3**, 1985: 1649
[70] Kubiak, G. D., Sitz, G. O., Zare R. N. *J. Chem. Phys.* **83**, 1984: 2538
[71] Zacharias, H., David, R., *Chem. Phys. Lett.* **115**, 1985: 205-8
[72] Schröter, L., Zacharias, H., David, R., *Phys. Rev. Lett.* **62**, 1989: 571
[73] Harris, J. E., Rahman, T., and Yang, K., *Surf. Sci.* **198**, 1988: 1312
[74] Müller, J. E., *Phys. Rev. Lett.* **59**, 1987: 2943
[75] Schröter, L., Zacharias, H., David, R., *J. Vac. Sci. Technol.* **A9**, 1991: 1712
[76] K. Yang and T. S. Rahman *J. Chem. Phys.* **93**, 1990: 6834
[77] Schröter, L., David, R., Zacharias, H., *Surf. Sci.* **258**, 1991: 259
[78] Schröter, L., Trame, Chr., David, R., Zacharias, H., *Surf. Sci.* **272**, 1992: 229
[79] Kolasinski, K.W., Shane, S.F., Zare R. N., *J. Chem. Phys.* **96**, 1992: 3995
[80] Shane, S.F., Kolasinski, K.W., Zare R. N., *J. Chem. Phys.* **97**, 1992: 3704
[81] Rinnen, K.-D., Buntine, M. A.,Kliner, D. A. V. Zare R. N. and Huo,W. M. , *J. Chem. Phys.* **95**, 1991: 214
[82] Chen, X. R.; Wagemann, K.; Wanner, J.; Brenig, W; Kuchenhoff, S, *Surf. Sci.* **224**, 1989: 570
[83] Wageman, K.; Chen, X. R.; Näger, U.; Wanner, J. Vacuum **41**, 1990: 733
[84] Näger, U.; Bracker, A.; Chen, X. R.; Jakob, P.; Wanner, J. *J. Phys. Chem.* **95**, 1991: 8376
[85] Alstrin, A. L.; Smilgys, R. V.; Strupp, P. G.; Leone, S. R., *J. Chem. Phys.* **97,** 1992: 6864
[86] Smilgys, R. V.; Leone, S. R. *J. Vac. Sci. Technol* **B8**, 1990: 416
[87] Doak, R. R.; Nguyen, D. B. *Phys. Rev. B* **41**, 1990: 3578
[88] D. A. Mantell, R.R. Cavanagh, D. S. King, *J. Chem. Phys.* **84**, 1986: 5131
[89] A. R. Burns, D. R. Dennison and E. B. Stechel, *Phys. Rev. B Cond. Matter* **40**, 1989: 9485
[90]A. R. Burns, E. B. Stechel, and D. R. Dennison, *Phys. Rev. Lett.* **58**, 1987: 250
[91] A. R. Burns, E. B. Stechel, and D. R. Dennison, *J. Vac. Sci. Technol.* **A8**, 1990: 2705
[92] A. R. Burns, E. B. Stechel, and D. R. Dennison, *Phys. Rev. B Cond. Matt.* **45**, 1992: 1373
[93] A. R Burns, T. M. Orlando, D. R. Jennison, *J. Vac. Sci. Technol.* **A9**, 1991: 1774
[94] R. Schwarzwald, A. Modl and T. J. Chuang, *Surf. Sci.* **242**, 1991: 437
[95] E. Hasselbrink, S. Jakubith, S. Nettesheim, M. Wolf, A. Cassuto, and G. Ertl, *J. Chem. Phys.* **92**, 1990: 3154
[96] R. O. Loo, H.-P. Haerri, G. E. Hall and P. L. Houston, *J. Chem. Phys.* **90**,1990: 4222
[97] J. A. Prybyla, T. F. Heinz, J. A. Misewich, M. M. T. Joy, and J. H. Glownia, *Phys. Rev. Lett.*, **64**, 1990: 1537
[98] F. Budde, T. F. Heinz, M. M. T. Joy, J. A. Misewich, F. de Rougemont and H. Zacharias, *Phys. Rev. Lett.*, **66**, 1991: 3024

[99] Kazuhiro Mase, et al , *J. Chem. Phys.* **96**, 1992: 5523
[100] Kazuhiro Mase, et al., *J. Chem. Phys.* **91**, 1989: 590
[101] Kazuhiro Mase, et al., *Surf. Sci.* **242**, 1991: 444
[102] Richter, Lee J., Buntin S. A., King D. S., Cavanagh, R. R., *J. of Electr. Spec. and Relat. Phen.* **54/55**, 1990: 181-90
[103] Weeks, J. D., Tully, J. C., Kimerling, L. C., *Phys. Rev. B* **12**, 1975: 3286
[104] Ying, Z. C. and Ho, W., *J. Chem. Phys.* **93**, 1990: 9089
[105] Richter, Lee J., Buntin S. A., King D. S., Cavanagh, R. R., *J. Chem. Phys.* **96**, 1992: 2324